Oda *et al. Earth, Planets and Space* (2016) 68:109
DOI 10.1186/s40623-016-0493-2

Earth, Planets and Space

TECHNICAL REPORT

Open Access

Toward robust deconvolution of pass-through paleomagnetic measurements: new tool to estimate magnetometer sensor response and laser interferometry of sample positioning accuracy

Hirokuni Oda[1*], Chuang Xuan[2] and Yuhji Yamamoto[3]

Abstract

Pass-through superconducting rock magnetometers (SRM) offer rapid and high-precision remanence measurements for continuous samples that are essential for modern paleomagnetism studies. However, continuous SRM measurements are inevitably smoothed and distorted due to the convolution effect of SRM sensor response. Deconvolution is necessary to restore accurate magnetization from pass-through SRM data, and robust deconvolution requires reliable estimate of SRM sensor response as well as understanding of uncertainties associated with the SRM measurement system. In this paper, we use the SRM at Kochi Core Center (KCC), Japan, as an example to introduce new tool and procedure for accurate and efficient estimate of SRM sensor response. To quantify uncertainties associated with the SRM measurement due to track positioning errors and test their effects on deconvolution, we employed laser interferometry for precise monitoring of track positions both with and without placing a u-channel sample on the SRM tray. The acquired KCC SRM sensor response shows significant cross-term of Z-axis magnetization on the X-axis pick-up coil and full widths of ~46–54 mm at half-maximum response for the three pick-up coils, which are significantly narrower than those (~73–80 mm) for the liquid He-free SRM at Oregon State University. Laser interferometry measurements on the KCC SRM tracking system indicate positioning uncertainties of ~0.1–0.2 and ~0.5 mm for tracking with and without u-channel sample on the tray, respectively. Positioning errors appear to have reproducible components of up to ~0.5 mm possibly due to patterns or damages on tray surface or rope used for the tracking system. Deconvolution of 50,000 simulated measurement data with realistic error introduced based on the position uncertainties indicates that although the SRM tracking system has recognizable positioning uncertainties, they do not significantly debilitate the use of deconvolution to accurately restore high-resolution signal. The simulated "excursion" event associated with a significant magnetization intensity drop was clearly recovered in the deconvolved measurements with a maximum error of ~3° in inclination.

Keywords: Superconducting rock magnetometer, Pass-through measurement, Sensor response, Deconvolution, Laser interferometry, Geomagnetic excursion, U-channel, Sediment long-core sample

Introduction

The development of pass-through superconducting rock magnetometers (SRM) has enabled continuous high sensitivity measurement of remanent magnetizations of sediments (e.g., Dodson et al. 1974; Goree and Fuller 1976; Weeks et al. 1993), leading to rapid accumulation of high-resolution paleomagnetic and environmental magnetic records. The continuous records acquired on pass-through SRMs, especially those with u-channels (Tauxe et al. 1983), have revolutionized paleomagnetism

*Correspondence: hirokuni-oda@aist.go.jp
[1] Institute of Geology and Geoinformation, Geological Survey of Japan, AIST, Central 7, 1-1-1 Higashi, Tsukuba 305-8567, Japan
Full list of author information is available at the end of the article

Springer Open

© 2016 The Author(s). This article is distributed under the terms of the Creative Commons Attribution 4.0 International License (http://creativecommons.org/licenses/by/4.0/), which permits unrestricted use, distribution, and reproduction in any medium, provided you give appropriate credit to the original author(s) and the source, provide a link to the Creative Commons license, and indicate if changes were made.

through reconstruction of paleomagnetic field at unprecedented resolution and scale (e.g., Valet and Meynadier 1993; Guyodo and Valet 1999; Valet et al. 2005; Roberts 2006; Ohno et al. 2008; Channell et al. 2009; Roberts et al. 2013) and greatly contributed to the paleomagnetic data archive based on sediments (Xuan and Channell 2009; Brown et al. 2015).

Continuous measurements on pass-through SRMs, however, are subjected to smoothing and distortion due to the convolution of sensor responses, controlled by the geometry of pick-up coils and superconducting shield, with the magnetization of paleomagnetic sample (e.g., Shibuya and Michikawa 2000; Oda and Xuan 2014). Deconvolution is needed to reconstruct higher-resolution magnetization time series with less distortion (e.g., Dodson et al. 1974; Constable and Parker 1991; Oda and Shibuya 1996; Guyodo et al. 2002; Jackson et al. 2010). Oda and Xuan (2014) recently developed an improved deconvolution algorithm based on ABIC minimization method considering realistic errors in sample length and measurement position. Based on the algorithm, standalone graphical software UDECON was developed to directly read pass-through measurement data and perform fast and reliable deconvolution optimization (Xuan and Oda 2015).

Accurate measurements of sensor response including cross-terms are required to conduct deconvolution (e.g., Parker and Gee 2002; Jackson et al. 2010; Oda and Xuan 2014). Oda and Xuan (2014) developed a practical tool to measure sensor response systematically on 5-mm-spacing grids in three orthogonal directions. However, it is possible to improve the efficiency, repeatability and accuracy of the sensor response measurements by better constraining the point source position relative to individual grids as the authors used a double-sided tape to fix the Point Source Cube on the guide block.

Based on repeated measurements of a u-channel sample, Oda and Xuan (2014) demonstrated that accuracy of the deconvolved magnetizations is significantly controlled by SRM measurement noises. However, we currently have little knowledge on the characteristics of noises on the SRMs. A main source of SRM measurement noise is the positioning error of SRM tracking system (e.g., Jackson et al. 2010; Oda and Xuan 2014), which could contaminate both sensor response and sample measurements.

In order to facilitate implementation of the UDECON software (Xuan and Oda 2015) and to further understand uncertainties associated with pass-through measurements and deconvolution, we present new tool and procedure for accurate and more efficient measurements of SRM sensor response and use laser interferometry to evaluate the positioning error of the SRM tracking system. The new tools and procedures were used to measure the sensor response of SRM at Kochi Core Center (KCC), Japan, one of the core repositories of International Ocean Discovery Program (IODP), to ensure better reproducibility and accuracy of point source positions on the grid with improved orthogonality of three-axes orientation of the magnetic point source. The laser interferometry-acquired sample tray positions were compared with stepping motor counts. We also discuss the characteristics of positions measured with laser interferometry and the positioning errors associated with the SRM track system as well as their potential influence on deconvolution.

Response function determination

SRM at KCC

Figure 1 shows a schematic view of the u-channel pass-through SRM system (2G Enterprises model 755R) at KCC. The flat sample tray is made of fiber-reinforced plastics and is placed on a track. Both ends of the tray are connected to the original thread provided by the SRM manufacturer (2G Enterprises). The thread is tied to a laddered plastic rope that is connected to a gear attached to a stepping motor. At each end of the track there are clockwise (CW) and counterclockwise (CCW) limit switches. The SRM system at KCC uses the 2G Long Core software (version 3.4) installed on a Windows PC for its operation. Sample Handler Utility included in the software allowed us to control the position of the sample tray on the track by driving the stepping motor at two different speeds (slow or fast).

Sensor response measurements

Oda and Xuan (2014) used a 5-mm plastic cube with a point source in the center (Point Source Cube hereafter) and a larger cube with 25 mm edge length and one surface having $5 \times 5 = 25$ marked grid points. The Point Source Cube was attached onto the grid point on the surface of the larger cube using double-sided tape (Fig. 1b in Oda and Xuan 2014). The orientation of Point Source Cube on the X- and Y-axes plane was controlled with a plastic rod, and orientation along the Z-axis depends on the flatness of the double-sided tape. Here, we use new tool and procedure to facilitate the precise measurements of sensor response for the SRM at KCC. We modified one surface of the larger cube to include 16 grid positions evenly distributed with 6 mm $\times$ 6 mm spacing, each of which has four surrounding plastic walls to accurately hold the Point Source Cube (Fig. 2a, b). Point Source Cube was placed to each of these grid positions to measure sensor response with magnetization orientation parallel to +X-, +Y- or +Z-axes. The measurement data collected at every 1-mm interval for 300 mm along

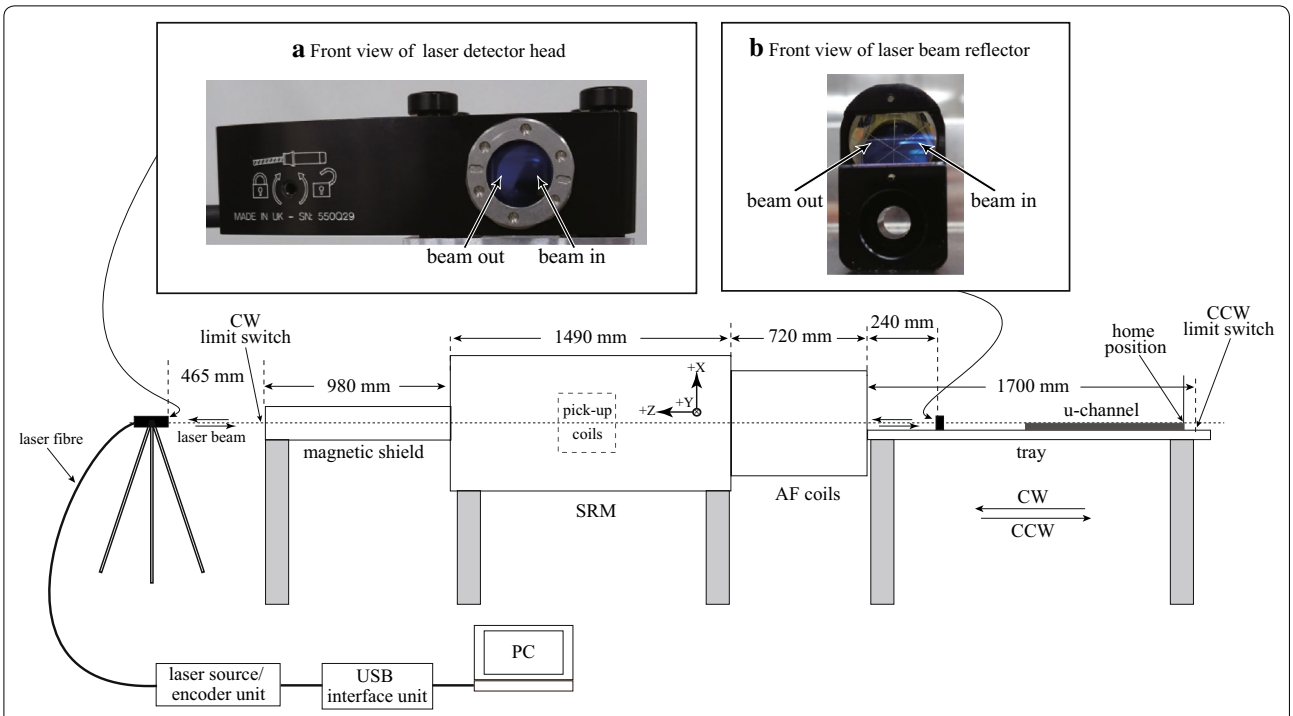

Fig. 1 Schematic diagram illustrating the setup for laser interferometry measurement. Laser beam is emitted from **a** the laser detector head, enters the bore of SRM from the side of CW limit switch, and is then reflected by **b** the laser beam reflector attached on the sample tray. Reflected laser beam goes back to the laser detector head through the bore of SRM, which is used for laser interferometry together with the source beam

the track were then interpolated (or extrapolated for the bottom grid points) into 1-mm grids from 6-mm measurement grids over the cross-sectional area of the larger cube surface. With the above grid data, integration was conducted over the cross-sectional area of a u-channel sample (i.e., horizontal = 18 mm; vertical = 19 mm; bottom height from the tray = 2 mm; centered along track).

Magnetic moment of the Point Source Cube was measured on a spinner magnetometer (Natsuhara Giken Co. Ltd.) at the Geological Survey of Japan. It has declination, inclination, and magnetic moment of 0.2°, 0.3°, and 5.30×10^{-7} Am^2, respectively.

KCC sensor response

Complete tensor components of sensor response curve for the u-channel SRM at KCC (KCC SRM sensor response) are shown in Fig. 2c. The three diagonal terms (i.e., "XX," "YY," and "ZZ" in Fig. 2c) of the KCC SRM sensor response tensor show single peaks with their full widths at half maxima (FWHM) of 46 mm (XX), 46 mm (YY), and 54 mm (ZZ). The positions of central maximum of XX, YY, and ZZ are −0.02, −0.04, and 0.07 mm, respectively. The XX and YY terms have negative lobes on both sides. There are also cross-terms between X- or Y-axis and Z-axis (i.e., XY, YX, XZ, and ZX). The prominent feature is that the ZX cross-term shows negative and positive peak values of ~25 % relative to the central peak value of the main ZZ term. This could be explained by the relatively large offset of the center of X-, Y-, and Z-coils relative to the center of u-channel about 8-mm downward (-X direction) for KCC sensor response, which is calculated by the X–Y position of minimum of peak values along Z-axis. The XY or YX terms are about 10 or 6 % of peak values in the XX or YY main terms, which could be minimized by rotating X-axis magnetization and Y-axis magnetization 4.5° counterclockwise along Z-axis (looking at SRM from the home position). This observation suggests that X–Y coil system is rotated 4.5° counterclockwise relative to the plane of tray and track.

Comparison and interpretation of sensor responses

The KCC SRM sensor response shows different shapes from that of SRM at Oregon State University (OSU SRM sensor response). Oda and Xuan (2014) reported that OSU SRM sensor response has FWHM of 80 mm (XX), 76 mm (YY), and 73 mm (ZZ) for the main terms, which are apparently 1.4–1.7 times wider than those of the KCC SRM sensor response. FWHM of XX or YY components

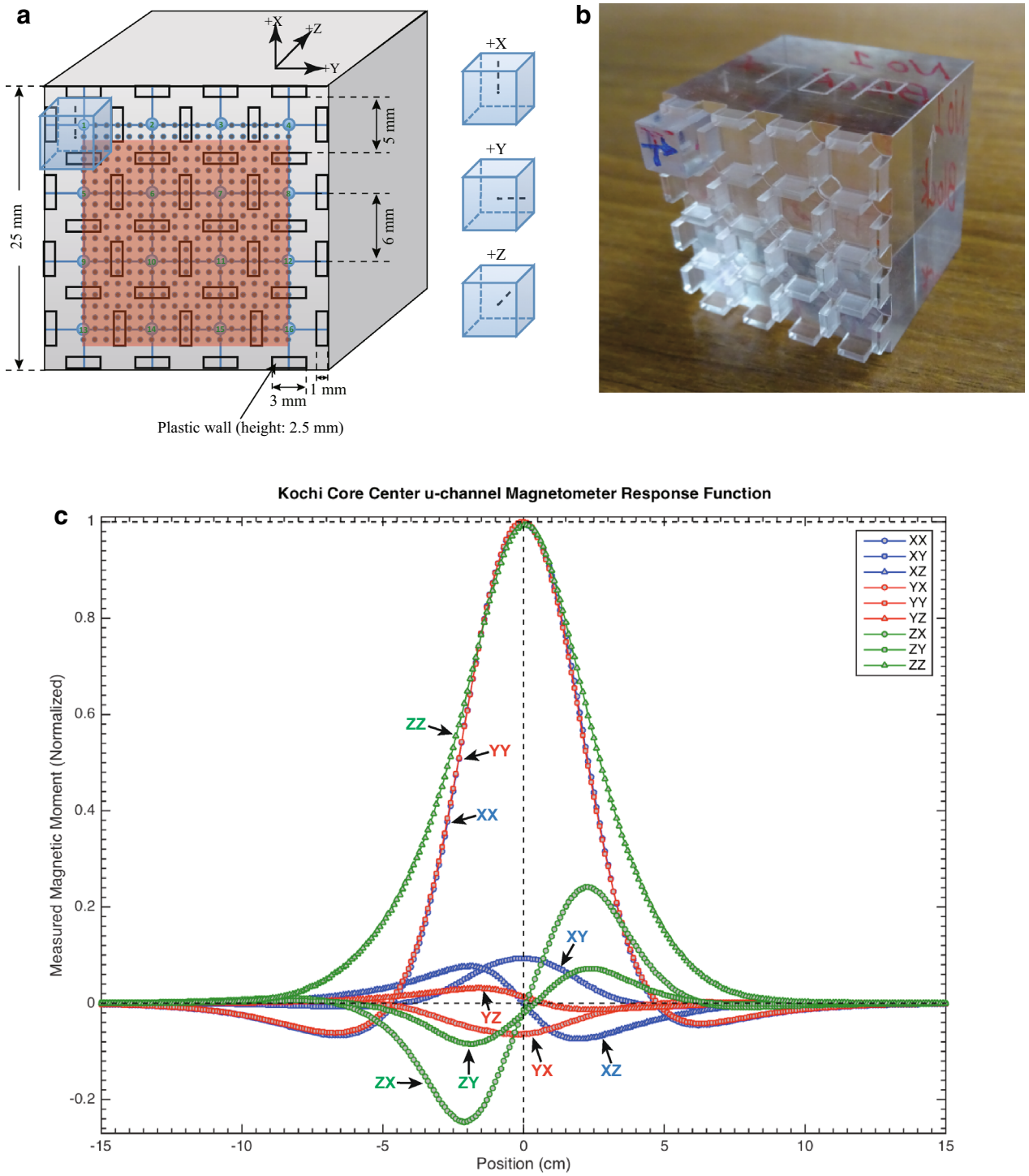

Fig. 2 **a** Schematic diagram of sensor response measurement tools. A plastic cube with edge length of 25 mm was used to hold the Point Source Cube during measurement. One surface of the cube has 4 × 4 grid positions, each of which has 5 mm × 5 mm *rectangular space* enclosed by four plastic walls with 3 mm width, 2.5 mm height, and 1 mm thickness. Point Source Cube can tightly fit in each of the 16 grid positions (numbered from 1 to 16). Each *small dot* corresponds to 1-mm-spacing grids. *Shading with orange color* shows the area corresponding to the cross section of a u-channel, which is used for integration. **b** A picture showing the actual plastic cube and Point Source Cube during a measurement on the KCC SRM. **c** Sensor response of SRM at KCC integrated over u-channel cross-sectional area at 1-mm interval along Z-axis. "AB" in legend means sensor response of "B"-axis pick-up coil to magnetization oriented along "A"-axis, where "A" and "B" are either "X," "Y," or "Z." Note relatively large ZX cross-term with anti-symmetry

are narrower than ZZ component for the KCC SRM sensor response, whereas opposite is true for the OSU SRM sensor response. Other features to note are that there is a single peak in the ZZ term for the KCC SRM sensor response, while the OSU SRM sensor response shows double peak separated ~20 mm from each other. In addition, XX and YY terms of the KCC SRM sensor response have negative lobes on both sides, whereas the OSU SRM sensor response has almost no such negative lobes.

These differences in the sensor responses could be caused by different designs between SRMs at KCC (cooled with liquid helium) and OSU (cooled with pulse tube). For instance, the KCC SRM pick-up coils may have narrower widths along the SRM track. Jackson et al. (2010) noted that the geometry of the superconducting shield in the "dry" SRM (cooled with pulse tube) is different from that in the conventional liquid He-cooled SRM, and the sensor response function is different accordingly. It is therefore critical to estimate the sensor response accurately for both types of SRM in order to successfully utilize the deconvolution. The narrow width of pick-up coils with narrow FWHM of KCC SRM sensor response is suitable for reconstruction of higher-resolution paleomagnetic signals with deconvolution.

Among the same type of SRMs, there are also some difference in sensor response functions. For example, SRM at OSU is a similar type to SRM at the Institute of Rock Magnetism (IRM), University of Minnesota. However, SRM at IRM has asymmetry with negative lobe on one side of sensor responses of XX and YY (Jackson et al. 2010). The asymmetry of SRM at IRM might have originated from the offset of center of the superconducting shield relative to the center of pick-up coils of X- and Y-axes.

Rotation of ~5° for X–Y pick-up coils relative to the plane of the tray seems to be a common feature of the 2G SRMs (e.g., Parker and Gee 2002; Jackson et al. 2010; Oda and Xuan 2014). This might be related to the construction of SRMs and/or the installation at the laboratories. 2G Enterprises documented the following in their Long Core v1.0 manual in 1996: "This misalignment angle can be determined by measuring a core once, then measuring it again after rotating the sample 180° about its +X axis." This description is not included in later versions of manual for the 2G Long Core software (e.g., v3.0 and v3.2).

Considering the fact that SRM users are not provided with the information on the geometry of pick-up coils and superconducting shield, rotation angle of X–Y pick-up coils, and sensor responses in real shape, it is necessary to estimate sensor responses accurately with a point source for each laboratory. An integrated sensor response can then be constructed for cross-sectional area corresponding to measured samples such as the u-channels. The new tool and procedure provide an effective approach in improving the efficiency and accuracy of sensor response curve estimates.

Laser interferometry of SRM tray position

Experimental setup of laser interferometry

Accurate positions of the SRM sample tray were measured with laser interferometry relative to the home position (-Z direction; see Fig. 1). The measurements were conducted using a laser encoder unit RLU10 (Renishaw plc) together with a laser detector head (RLD 90° RRI), a laser beam reflector (RLR10-A3-XF), and a USB interface unit (RSU10). The laser encoder unit was connected to a PC with the USB interface unit, and the interferometry was conducted with a positioning accuracy measurement software provided by Renishaw plc.

The laser detector head (Fig. 1a) was attached on an adjustable support, fixed on a stable tripod, and placed ~465 mm behind the CW limit switch of the SRM system. The laser beam reflector (Fig. 1b) was mounted on a small adjustable support and firmly attached to the sample tray using double-sided tape. Laser beam generated from the laser encoder unit is transmitted through a laser fiber to the laser detector unit. It was then emitted from the laser detector passing through SRM and reflected with the laser beam reflector attached to the sample tray. The reflected laser beam was received with the detector head, which was used for the interference measurements together with the source laser beam. Approximate distance between the laser detector head and the laser beam reflector when the tray is at the home position was measured as ~3895 mm.

Alignment of laser beam was conducted with special care using the tripod and the adjustable support while observing the beam on a paper guide attached on the laser beam reflector at the home and CW limit switch positions. The final adjustments were made with the software by maximizing output signal of the interferometry. Each of the laser interferometry measurements was conducted relative to the home position at a sampling frequency of 1 kHz. Environmental corrections were conducted for all measurements with temperature of 23.5 °C, humidity of 40 %, and atmospheric pressure of 101.45 kPa. Static measurements without motion of the tray show a standard deviation of 0.7 μm, possibly due to background mechanical vibrations and variability of environmental parameters.

The laser interferometry was conducted in two directions of the tray movements, i.e., toward (CW direction) or away (CCW direction) from the SRM, at two speeds (slow or fast) with or without a sample. The stepping motor was driven incrementally by manual operation with 100 stepping motor counts (corresponding to

4.78 mm for KCC SRM) either in a manner that the tray moved toward or away from the SRM, while the laser interferometry data were being collected. The positions measured with laser interferometry were recorded and compared with the distance expected from the stepping motor counts. Table 1 summarizes laser interferometry measurements conducted, while the tray is moving with and without a sample. A 1020-mm-long u-channel filled with sediment (weight: 770 g) was used for laser interferometry measurements with sample.

SRM tray position measured with laser interferometry

When no sample was placed on the tray (a u-channel sample was placed on the tray), continuous measurements of laser interferometry were successful up to about 600 (200) mm from the home position, where signal suddenly became weaker than the threshold for continuous tracking of interference. The difficulty of laser beam tracking beyond a few tens of cm could be related to irregularities (or "topography") of the SRM track.

We started the collection of measurements either from the home position (CW; toward SRM) or from the position where the previous measurements were terminated due to poor interference signal (CCW; away from SRM). The tray movement was controlled by manually clicking the "Move" button in the Sample Handler Utility of the 2G Long Core software. Figure 3 shows the position, speed, and acceleration of the tray for laser interferometry measurements with (right) and without (left) a u-channel sample. In order to visualize the details, horizontal axis was expanded for data collected within the first ~2 s and is plotted in Fig. 4. The peak amplitude of the vibration is ~200 μm without the sample (Fig. 4a) and ~50 μm with the sample (Fig. 4b). Vibration of the tray position settles down after ~0.6 s without the sample and after ~0.4 s with the sample. Average speed of the tray without the sample is ~50 mm/s (Fig. 4a, middle panel) both for slow and for fast modes. The speed of the tray with the sample is also centered about 50 mm/s (Fig. 4b, middle panel). It seems that the speed of the tray has no significant influence on the position difference.

Positions of the SRM tray at KCC measured with laser interferometry were compared with those expected from the corresponding stepping motor counts, and the differences between the two (position difference) are plotted against the latter in Fig. 5. The position acquired by laser interferometry for each "move" was calculated by averaging laser interferometry data for a 200-ms time interval right before the next "move" (shaded area in Fig. 4). The differences without sample in the direction toward SRM (CW direction; Fig. 5a) from stepping motor count are within −0.4 to 0.3 mm for the entire 600-mm measured interval. It is notable that the position differences show comparable patterns in addition to random noises (Fig. 5a). Histograms of the position differences (Fig. 6a) show distributions with means between −0.12 and 0.05 mm and fairly consistent standard deviations between 0.10 and 0.12 mm.

The position differences without sample in the direction away from SRM (CCW direction; Fig. 5b) show a gap between the first measurement (reference position for laser interferometry, which is always zero) and the second measurement (the position after the first move) away from the tray. This feature may imply a backlash related to change in the direction of stepping motor motion. Similar to that observed for CW measurements, fluctuation of the position differences shows comparable pattern on position length scales of >a few centimeters for all four measurements (note that Run #12_2 or Run #14_2 is the continuation of Run #12 or Run #14 after recovery of laser tracking). Histograms of the position differences (Fig. 6b) show distributions with means between −0.35 and 0.12 mm and standard deviations between 0.08 and 0.15 mm. The dominating negative means for the runs

Table 1 List of measurements for laser interferometry

Run #	With/without U-channel	CW/CCW	Measured length (mm)
7	Without U-channel	CW	568.8
8	Without U-channel	CCW	616.6
9	Without U-channel	CW	568.8
10	Without U-channel	CCW	607.1
11	Without U-channel	CW	425.4
12	Without U-channel	CCW	358.5
12_2[a]	Without U-channel	CCW	262.9
13	Without U-channel	CW	568.8
14	Without U-channel	CCW	282.0
14_2[a]	Without U-channel	CCW	243.8
15	With U-channel	CW	90.8
16	With U-channel	CW	90.8
17	With U-channel	CW	109.9
18	With U-channel	CW	105.2
19	With U-channel	CCW	138.6
20	With U-channel	CW	105.2
21	With U-channel	CCW	129.1
22	With U-channel	CW	224.7
23	With U-channel	CCW	248.6
25	With U-channel	CW	229.4
26	With U-channel	CCW	253.3

Run #1 through #6 are test runs without appropriate setup of temperature, humidity, and pressure and discarded. Run #24 is a static measurement for the measurement of ambient noise

CW clockwise, *CCW* counterclockwise

[a] Measurements restarted after loosing track of laser

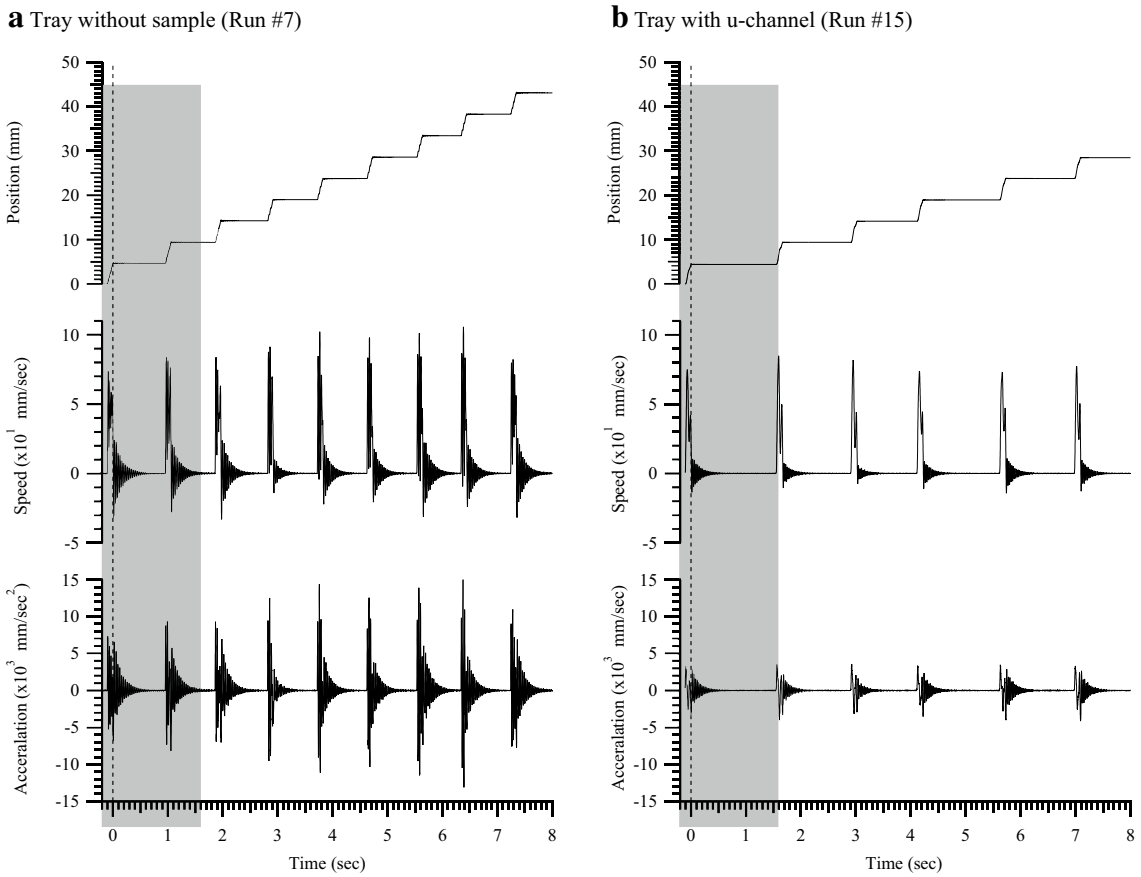

Fig. 3 Examples of precise measurement of position (*upper*), speed (*middle*), and acceleration (*bottom*) versus time for the tray of SRM at KCC using laser interferometry **a** without (Run #7) and **b** with (Run #15) a u-channel sample on the tray. *Vertical shading* is the interval shown in Fig. 4. Time is set as zero for the first trigger point (sharp drop in speed). The diagram shows only first nine or six stop positions out of a total of 19–119 positions

in CCW directions might be due to backlash mentioned above.

Although the records with sample were obtained for shorter intervals, the calculated position differences are between −0.3 and 0.9 mm for the total move of 250 mm in the direction toward SRM (CW direction; Fig. 5c) and are between −0.7 and 0.3 mm away from SRM (CCW direction; Fig. 5d). A significant increase of ~0.5 mm in the position differences was observed at position ~100 mm for the two runs toward SRM (CW direction; Fig. 5c). This might be related to the irregularity of the stepping motor belt or the roughness (or "topography") of the track surface. The histograms for the runs in CW direction (Fig. 6c) show distributions with means between 0.02 and 0.44 mm and standard deviations between 0.11 and 0.24 mm. The position differences calculated for the runs in the CCW direction (Fig. 6d) show distributions with means between −0.19 and 0.35 mm and standard deviations between 0.11 and 0.15 mm.

Positioning error of SRM track

The gap observed in multiple laser interferometry measurements conducted while moving the tray away from the SRM (CCW direction; Fig. 5b), possibly due to a backlash of the stepping motor, could be accounted for by the new parameter "position shift" introduced to the optimized deconvolution by Oda and Xuan (2014). The reason why such gap is absent in the CW direction measurements (e.g., Figure 5a) might be because the measurement in this direction starts from the home position, which is always calibrated through an initial move from the CCW limit switch (Fig. 1).

The positioning error of measurements on a SRM depends on the configuration in each laboratory. The source of stochastic errors observed in Fig. 5 might be random errors originating from the combination of multiple components of the tracking system (i.e., stepping motor, handler rope, pulley, and tray). Based on repeated measurements of a 1.5-m-long u-channel sample, Oda and Xuan (2014) estimated >0.06-mm positioning error

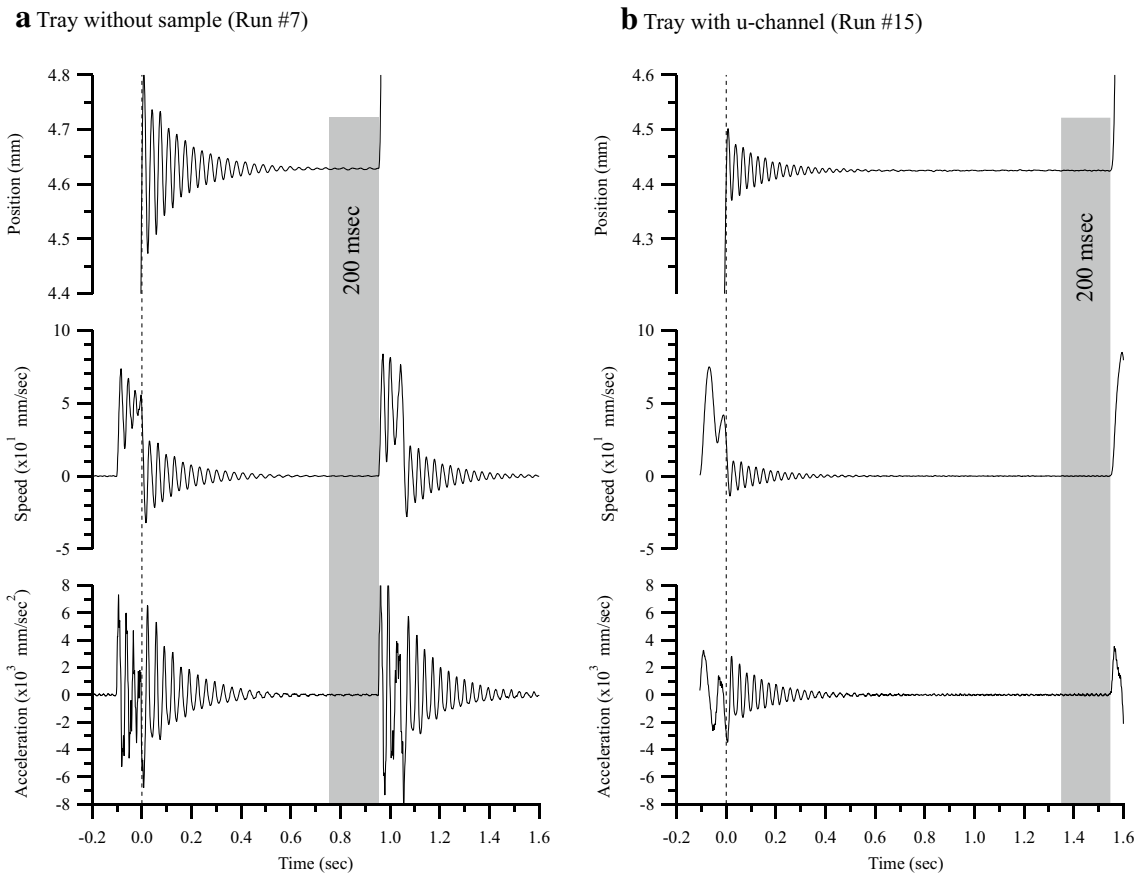

Fig. 4 Details of precise position (*upper*), speed (*middle*), and acceleration (*bottom*) versus time for the tray of SRM at KCC measured using laser interferometry **a** without (Run #7) and **b** with (Run #15) u-channel sample on the tray shown in Fig. 3. *Vertical shading* (200 ms before each move) is the interval used to calculate average positions in Fig. 5

for the SRM at OSU. It should be noted that the positioning error estimated from the standard deviation of repeated pass-through measurement is not absolute error but deviation from the average measurement at each position.

The first direct precise measurement of tray positions with laser interferometry conducted in this study revealed repeatable fluctuations (on length scales of >a few centimeters) in positioning of the SRM track system, which might be related to the condition of the various components of the track system (e.g., track or laddered rope). The apparently repeatable large position error of ~0.5 mm observed at ~100 mm for the measurements with u-channel samples (in CW direction, Fig. 5c) may need to be accounted for to achieve better deconvolution results. It should be noted that the repeatable stepwise positioning error could influence all the demagnetization steps and better to be avoided.

Figure 7a shows a histogram of position difference distribution calculated with all laser interferometry measurements in both CW and CCW directions, while no sample was placed on the tray. The average of the distribution is −0.12 mm with a standard deviation of 0.18 mm. The distribution for all laser interferometry measurements with a u-channel sample has average of 0.11 mm with a standard deviation of 0.27 mm (Fig. 7b). It appears that standard deviation of the position difference is larger for the measurements with a u-channel sample on the tray.

Deconvolution experiments using simulated data with positioning error

In order to investigate the effect of the observed positioning error on deconvolution, we conducted optimized deconvolution experiments 50,000 times using synthetic data with realistic position errors. Synthetic "ideal" measurements were first produced by convolving a synthetic magnetization signal that contains an "excursion" event used by Oda and Xuan (2014) with the KCC SRM sensor response. We then introduced random position

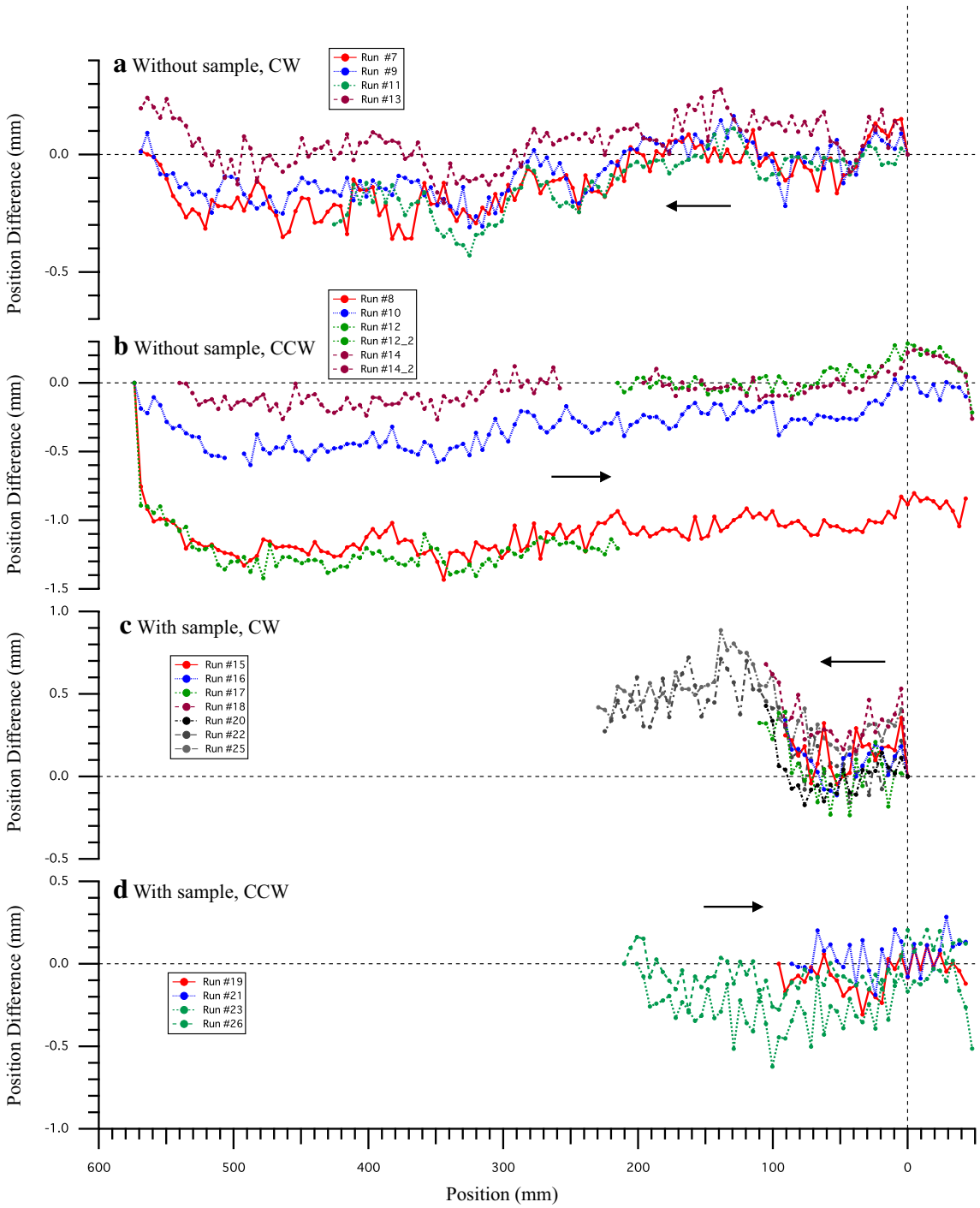

Fig. 5 Position difference (expected from stepping motor counts—position measured with laser interferometry) without u-channel sample on the tray for **a** clockwise (CW) and **b** counterclockwise (CCW) moving directions. Similarly, position difference with u-channel sample on the tray is shown in **c**, **d** for CW and CCW moving directions, respectively

errors to the KCC SRM sensor response data according to the histogram of position difference distribution acquired from the laser interferometry measurements, while no sample was placed on the tray (Fig. 7a). Similarly, at each sample measurement position, a random position error was introduced based on the histogram of

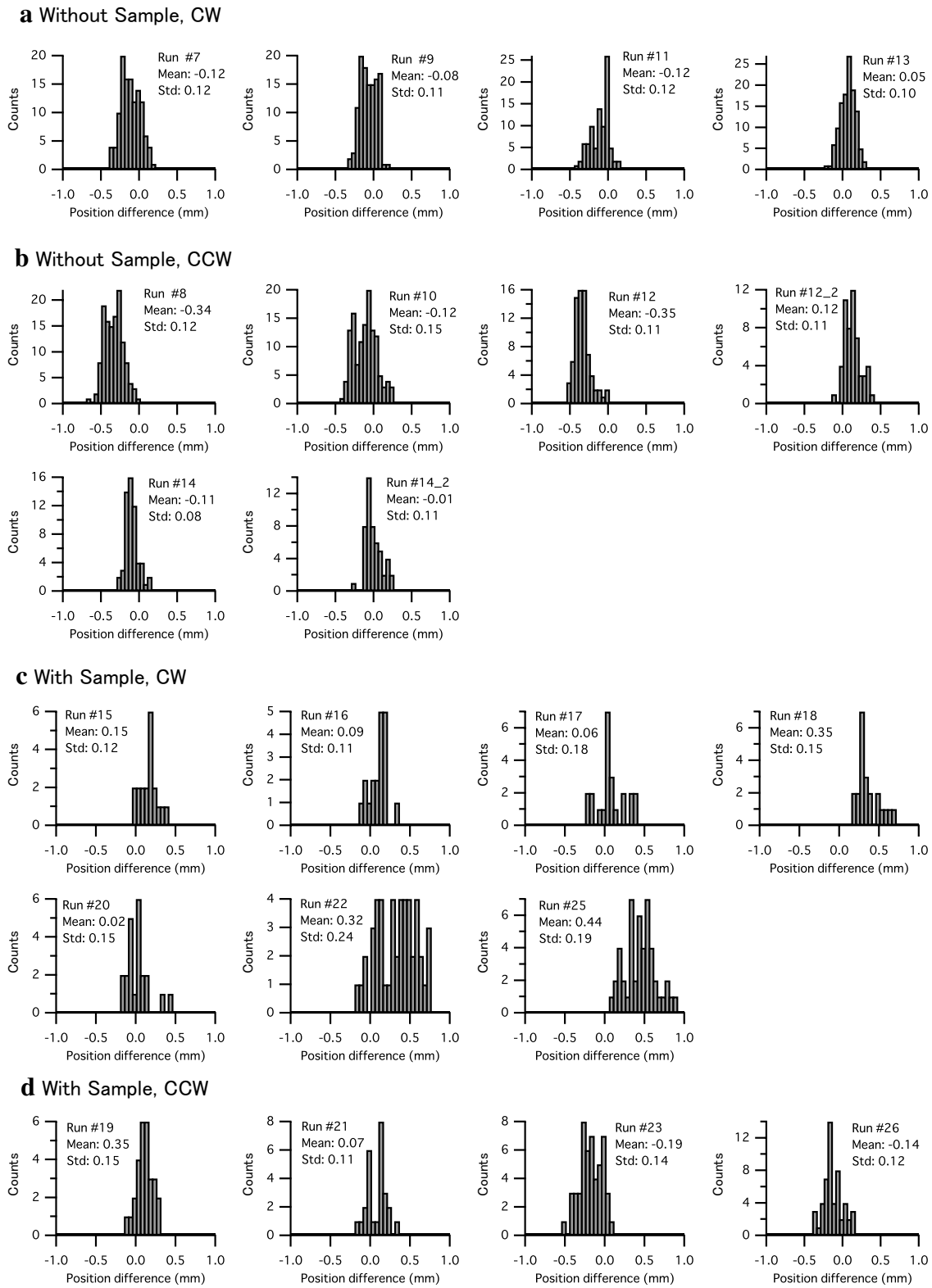

Fig. 6 Histograms of the position difference for individual laser interferometry runs listed in Table 1. **a** Runs in CW direction without sample on the tray, **b** runs in CCW direction without sample on the tray, **c** runs in CW direction with sample on the tray, and **d** runs in CCW direction with sample on the tray. *Each diagram* shows frequency versus position difference, which is accompanied by run number, mean, and standard deviation (Std) in mm

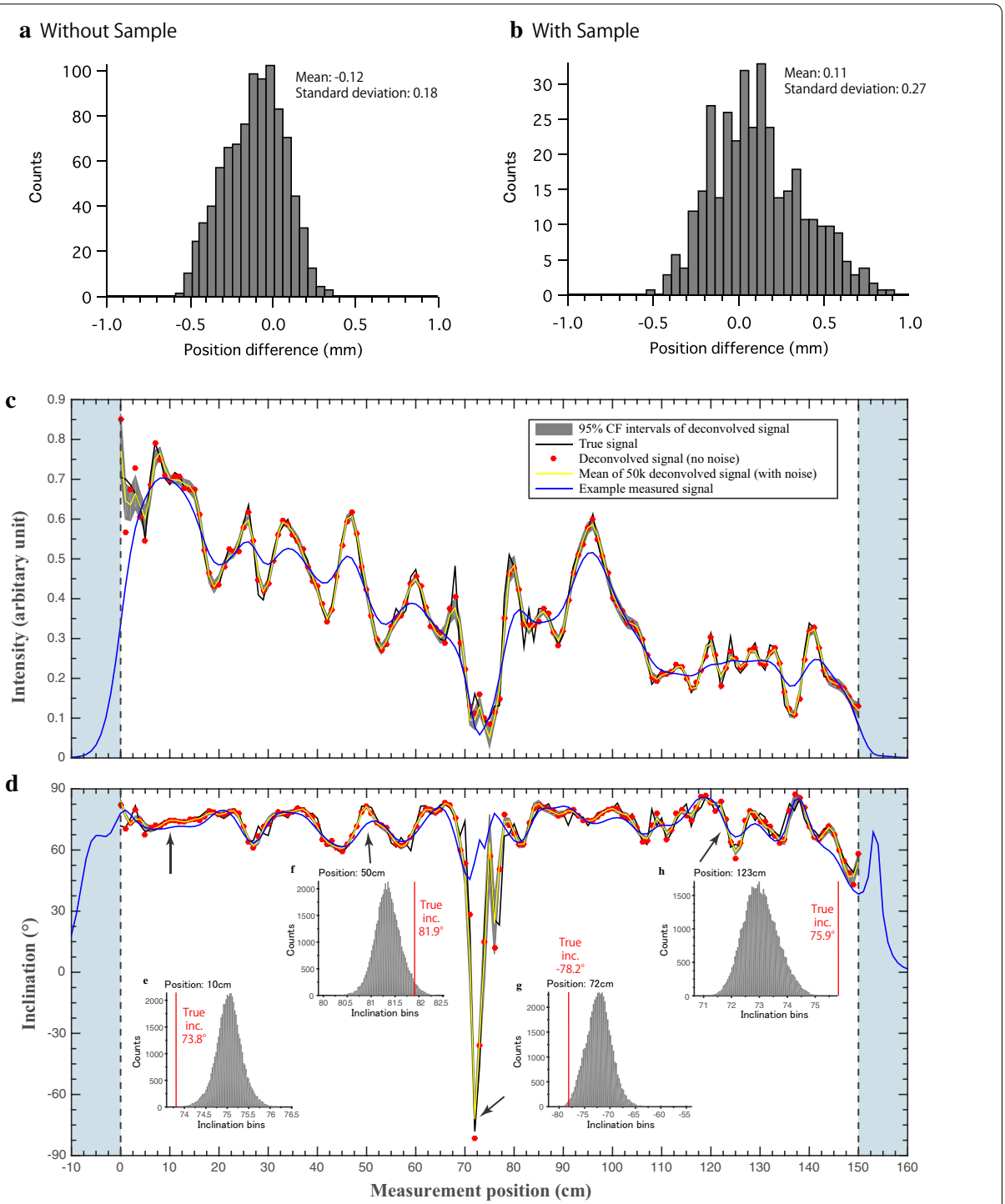

Fig. 7 **a** Histogram of all position differences from measurements in CW and CCW directions without u-channel sample on the tray. **b** Histogram of all position differences from measurements in CW and CCW directions with u-channel sample on the tray. Simulation results for **c** intensity and **d** inclination data. *Solid black curve* is true signal used to produce synthetic measurement, and *blue curve* is example of a measured signal with position errors added. *Red dots* are deconvolved signal using measurement and response function data without adding positioning errors. *Yellow curves* are mean of 50,000 deconvolved signals using measurement and response data with realistic positioning errors added. The *gray shading* represents 95 % confidence intervals of the deconvolved data. *Insets* in **d** are histograms of inclination for 50,000 deconvolved signals at *e* 15 cm, *f* 50 cm, *g* 72 cm, and *h* 123 cm positions, respectively. *Red vertical lines* represent true inclination values for the four positions

position differences acquired from the laser interferometry measurements with a u-channel sample on the tray (Fig. 7b). For both sensor response and synthetic sample measurement data, signal with positions at regular interval of 1 cm was used for the simulations. For each simulation the "ideal" measurement and response function data were resampled by spline interpolation based on positions displaced by adding random positioning errors. The measurement and response function resampled from the displaced positions were used for deconvolution as if the positions were not displaced.

The intensity and inclination data from the simulations are shown in Fig. 7c, d. Solid black curve is the true signal (artificial magnetization data set) used to produce synthetic measurements. An example of synthetic measurement is shown in blue curves, which was produced by convolving the true signal with the sensor response. Compared with the true signal, the measured signal shows significant smoothing and distortion due to the convolution effect of the pass-through system. SRM at KCC cannot successfully resolve the ~8-cm-long "excursion" event in the original true signal. In Fig. 7c, d, red dots are deconvolved data using measurement and response function data without adding any position errors. Mean (yellow curve) and the 95 % confidence intervals (shaded area) for all simulated deconvolution data (a total of 50,000 times) using the both measurement and response function data with realistic position errors suggest that deconvolution can successfully restore the true signal (both in amplitude and in direction) overcoming majority of the smoothing and distortion caused by the convolution effect. The "excursion" event was clearly recovered in the deconvolved measurements. Examples of histograms of inclination for 50,000 deconvolved signal show Gaussian-like distributions with standard deviations of ~0.3°, ~0.3°,~3°, and ~0.8° for positions at 15, 50, 72, and 123, respectively. A prominent evidence is that the midpoint of "excursion" with true inclination of −78.2° at 72 cm could be recovered successfully with relatively small uncertainty, which demonstrates the effectiveness of ABIC-minimizing deconvolution for measurement and response function data with realistic position errors.

Conclusions

New practical tool and procedure were developed to facilitate rapid and accurate measurements of SRM sensor response. Systematic measurements of Point Source Cube on SRM at KCC, Japan, were used to produce an accurate estimate for the sensor response, which can be used for deconvolution of u-channel pass-through measurements made on the SRM at KCC. A possible 4.5° counterclockwise rotation (looking at SRM from the home position) of the X–Y coil system relative to the Z-axis and significant ZX cross-term components were observed. As one of the main research facilities associated with the core repositories of the IODP, the SRM at KCC plays an important role in the collection of critical pass-through data for paleomagnetism research. The accurate estimate of sensor response function of the SRM at KCC, therefore, provides a valuable tool with broader impact to restore high-resolution signals for measurements through deconvolution.

Accurate measurements of SRM tray positions were conducted with and without a 1020-mm-long sediment u-channel at intervals of 4.78 mm using laser interferometry. Position vibrations were observed in all measurements following the stop of the tray movement. Measurements without (with) u-channel show vibrations with peak amplitudes of ~200 μm (~50 μm), which diminishes in ~0.6 s (~0.4 s). Comparison with the position expected from the stepping motor counts indicates random discrepancies with standard deviations of ~0.1–0.2 mm. Large gaps were observed just after the change in the direction of the stepping motor, which might be related to backlash of the stepping motor. Stepwise change of ~0.5 mm was recognized for measurements with u-channel sample on the tray, presumably due to the condition of the tray. Positioning error is larger with u-channel sample. Reproducible features in the position differences suggest influence of track/rope shapes on individual positions. Positioning error is generally between 0.06 and 1 mm. Although the current positioning system is accurate enough to reproduce 8-cm-long "excursion" event, it is recommended to build tray tracking system with better positioning accuracy to improve the pass-through measurements and performance of optimized deconvolution for higher resolution and accuracy.

We have conducted deconvolution experiments using synthetic data with realistic position errors acquired from the laser interferometry measurements. Synthetic measurement data were produced by convolving synthetic magnetization signal that includes an "excursion" event with the sensor response measured for KCC SRM. For both measurements and sensor response, positioning errors were randomly introduced based on the laser interferometry measurements conducted in this study. Deconvolution using the synthetic measurement data and response function estimates for SRM successfully restored the true signal overcoming majority of the smoothing and distortion caused by the convolution effect. The "excursion" event was clearly recovered in the deconvolved measurements with a maximum error angle of ~3°.

Abbreviations
ABIC: Akaike's Bayesian Information Criterion; AF: alternating field; CW: clockwise; CCW: counterclockwise; FWHM: full widths at half maxima; IODP: International Ocean Discovery Program; IRM: Institute of Rock Magnetism; KCC: Kochi Core Center; OSU: Oregon State University; SQUID: superconducting quantum interference device; SRM: superconducting rock magnetometer.

Authors' contributions
HO designed the experiments and wrote and edited most of the manuscripts. CX contributed to the calculation of sensor response and deconvolution with simulated data and wrote and edited the manuscript. YY provided the facility and helped the experiments and edited the manuscript. All authors read and approved the final manuscript.

Author details
[1] Institute of Geology and Geoinformation, Geological Survey of Japan, AIST, Central 7, 1-1-1 Higashi, Tsukuba 305-8567, Japan. [2] School of Ocean and Earth Science, National Oceanography Centre Southampton, University of Southampton, Waterfront Campus, European Way, Southampton SO14 3ZH, UK. [3] Center for Advanced Marine Core Research, Kochi University, B200 Monobe, Nankoku, Kochi 783-8502, Japan.

Acknowledgements
Hirokuni Oda was supported by JSPS Grant-in-Aid for Scientific Research (A) Funding Nos. 25247082 and 25247073. Chuang Xuan is supported by a startup fund provided by the University of Southampton. JSPS provided a Visiting Fellowship for Foreign Researchers (Award No. PE14034) for Chuang Xuan to visit Geological Survey of Japan (GSJ), National Institute of Advanced Industrial Science and Technology (AIST), to conduct work related to this research. This study was performed under the cooperative research program of Center for Advanced Marine Core Research (CMCR), Kochi University (Accept Nos. 14B040 and 15A048). Part of the measurements was conducted with facilities of *GSJ-Lab.*, and a plastic block for the point source was fabricated with the help of Tomomi Kobayashi at AIST. The authors would like to thank Ayako Katayama at AIST who helped the production of figures. The study could not be completed without the construction of SRMs provided by 2G Enterprises, especially the pioneering works by William S. Goree.

Competing interests
The authors declare that they have no competing interests.

Received: 8 April 2016 Accepted: 15 June 2016
Published online: 08 July 2016

References

Brown MC, Donadini F, Nilsson A, Panovska S, Frank U, Korhonen K, Schuberth M, Korte M, Constable CG (2015) GEOMAGIA50.v3: 2. A new paleomagnetic database for lake and marine sediments. Earth Planets Space 67:70. doi:10.1186/s40623-015-0233-z

Channell JET, Xuan C, Hodell DA (2009) Stacking paleointensity and oxygen isotope data for the last 1.5 Myr (PISO-1500). Earth Planet Sci Lett 283:14–23. doi:10.1016/j.epsl.2009.03.012

Constable C, Parker R (1991) Deconvolution of longcore palaeomagnetic measurements—spline therapy for the linear problem. Geophys J Int 104:453–468. doi:10.1111/j.1365-246X.1991.tb05693.x

Dodson RE, Fuller MD, Pilant W (1974) On the measurement of the remanent magnetism of long cores. Geophys Res Lett 1:185–188. doi:10.1029/GL001i004p00185

Goree WS, Fuller MD (1976) Magnetometers using RF-driven SQUIDs and their applications in rock magnetism and paleomagnetism. Rev Geophys Space Phys 14:591–608

Guyodo Y, Valet JP (1999) Global changes in intensity of the Earth's magnetic field during the past 800 kyr. Nature 399:249–252. doi:10.1038/20420

Guyodo Y, Channell JET, Thomas RG (2002) Deconvolution of u-channel paleomagnetic data near geomagnetic reversals and short events. Geophys Res Lett 29:1845. doi:10.1029/2002GL014927

Jackson M, Bowles JA, Lascu I, Solheid P (2010) Deconvolution of u channel magnetometer data: experimental study of accuracy, resolution, and stability of different inversion methods. Geochem Geophys Geosyst 11:Q07Y10. doi:10.1029/2009GC002991

Oda H, Shibuya H (1996) Deconvolution of long-core paleomagnetic data of Ocean Drilling Program by Akaike's Bayesian Information Criterion minimization. J Geophys Res 101:2815–2834. doi:10.1029/95JB02811

Oda H, Xuan C (2014) Deconvolution of continuous paleomagnetic data from pass-through magnetometer: a new algorithm to restore geomagnetic and environmental information based on realistic optimization. Geochem Geophys Geosyst 15:3907–3924. doi:10.1002/2014GC005513

Ohno M, Murakami F, Komatsu F, Guyodo Y, Acton G, Kanamatsu T, Evans HF, Nanayama F (2008) Paleomagnetic directions of the Gauss–Matuyama polarity transition recorded in drift sediments (IODP Site U1314) in the North Atlantic. Earth Planets Space 60:e13–e16

Parker RL, Gee JS (2002) Calibration of the pass-through magnetometer-II. Application. Geophys J Int 150:140–152. doi:10.1046/j.1365-246X.2002.01692.x

Roberts AP (2006) High-resolution magnetic analysis of sediment cores: strengths, limitations and strategies for maximizing the value of long-core magnetic data. Phys Earth Planet Inter 156:162–178. doi:10.1016/j.pepi.2005.03.021

Roberts AP, Tauxe L, Heslop D (2013) Magnetic paleointensity stratigraphy and high-resolution Quaternary geochronology: successes and future challenges. Quat Sci Rev 61:1–16

Shibuya H, Michikawa T (2000) Calculation of superconducting rock magnetometer response. Kumamoto J Sci Earth Sci 16:1–16

Tauxe L, Labrecque JL, Dodson D, Fuller M (1983) "U" channels—a new technique for paleomagnetic analysis of hydraulic piston cores. EOS Trans Am Geophys Union 64:219

Valet JP, Meynadier L (1993) Geomagnetic field intensity and reversals during the past four million years. Nature 366:234–238. doi:10.1038/366234a0

Valet JP, Meynadier L, Guyodo Y (2005) Geomagnetic dipole strength and reversal rate over the past two million years. Nature 435:802–805. doi:10.1038/nature03674

Weeks R, Laj C, Endignoux L, Fuller M, Roberts A, Manganne R, Blanchard E, Goree W (1993) Improvements in long-core measurement techniques: applications in palaeomagnetism and palaeoceanography. Geophys J Int 114:651–662

Xuan C, Channell JET (2009) UPmag: MATLAB software for viewing and processing u-channel or other pass-through paleomagnetic data. Geochem Geophys Geosyst 10:Q10Y07. doi:10.1029/2009GC002584

Xuan C, Oda H (2015) UDECON: deconvolution optimization software for restoring high-resolution records from pass-through paleomagnetic measurements. Earth Planets Space 67:183. doi:10.1186/s40623-015-0332-x

Submit your manuscript to a SpringerOpen journal and benefit from:

- ► Convenient online submission
- ► Rigorous peer review
- ► Immediate publication on acceptance
- ► Open access: articles freely available online
- ► High visibility within the field
- ► Retaining the copyright to your article

Submit your next manuscript at ► springeropen.com